Double-slit interference of single twisted photons

Wen-Rong Qi (齐文荣)[1], **Rui Liu** (刘 瑞)[1], **Ling-Jun Kong** (孔令军)[2], **Zhou-Xiang Wang** (王周祥)[1], **Shuang-Yin Huang** (黄双印)[1], **Chenghou Tu** (涂成厚)[1], **Yongnan Li** (李勇男)[1,*], **and Hui-Tian Wang** (王慧田)[2,**]

[1]*Key Laboratory of Weak-Light Nonlinear Photonics and School of Physics, Nankai University, Tianjin 300071, China*
[2]*National Laboratory of Solid State Microstructures, School of Physics, and Collaborative Innovation Center of Advanced Microstructures, Nanjing University, Nanjing 210093, China*
**Corresponding author: liyongnan@nankai.edu.cn; **corresponding author: htwang@nju.edu.cn*
Received May 10, 2020; accepted June 1, 2020; posted online July 30, 2020

Optical orbital angular momentum (OAM) is a special property of photons and has evoked research onto the light–matter interaction in both classical and quantum regimes. In classical optics, OAM is related to an optical vortex with a helical phase structure. In quantum optics, photons with a twisted or helical phase structure will carry a quantized OAM. To our knowledge, however, so far, no experiment has demonstrated the fundamental property of the OAM at the single-photon level. In this Letter, we have demonstrated the average photon trajectories of twisted photons in a double-slit interference. We have experimentally captured the double-slit interference process of twisted photons by a time-gated intensified charge-coupled device camera, which is trigged by a heralded detection. Our work provides new perspectives for understanding the micro-behaviors of twisted particles and enables new applications in imaging and sensing.

Keywords: orbital angular momentum; double-slit interference; twisted photons; helical phase.
doi: 10.3788/COL202018.102601.

Recently, an essential quantum feature of photons is the fact that it can carry orbital angular momentum (OAM)[1], which has attracted a lot of attention in classical[2,3] and quantum optics[4]. In classical optics, OAM is related to an optical vortex with a helical phase structure of $\exp(i\ell\phi)$ (ℓ is the topological charge). This helical phase wraps around the axis of propagation ℓ times, which results in a phase singularity at the beam center. For the first time, to the best of our knowledge, it has been observed that light with a twisted structure travels slower than the established speed of light[5]. In quantum optics, photons with a twisted or helical phase structure of $\exp(i\ell\phi)$ will carry a quantized OAM of $\ell\hbar$ ($\hbar$ is the reduced Planck constant) per photon, providing an infinite-dimensional Hilbert space[4]. Therefore, high-dimensional quantum information can be stored in the OAM of single photons, which holds great potential for quantum computing[6] and communication[7] applications. As a new and important degree of photons, how to understand the wave and particle characters of OAM is a fundamental issue and a basis of the potential application.

The double-slit interference devised by Thomas Young plays an important role in physics and strikingly demonstrates the wave-particle duality of quantum objects. Such an experiment can be performed with particles ranging from individual photons[8,9], electrons[10], neutrons[11], and atoms[12], to large molecules consisting of dozens of atoms[13]. Some counterintuitive features such as entanglement, non-locality, wave-particle duality, and delayed-choice concepts can be demonstrated or tested using a double-slit configuration[14–21]. Entanglement between the wave and particle states of two photons has been proved, which opens the way for potential applications of quantum information protocols to encode qubits by exploiting the wave-particle degree of freedom[22]. However, double-slit interference of twisted photons carrying OAM at the single-photon level has not been reported yet.

In this Letter, we have demonstrated the average photon trajectories (APTs) of twisted photons carrying OAM in Young's double-slit interference. Kocsis *et al.*[18] measured the APTs of single photons in a double-slit configuration by using the technique of quantum weak measurements[23]. Later, it appears that weak measurements of the local momentum of photons made by Kocsis *et al.* represent measurements of the Poynting vector in an optical field[24]. This arouses our interest in the study of the APTs of twisted photons. We carry out Young's double-slit interference with single twisted photons based on a triggered intensified charge-coupled device (ICCD), because the coincidence image can greatly degrade noise. Photons pass one by one through a pair of slits, where single photons from a given slit can be detected (particle-like character). The interference fringes emerge (wave-like character) on a screen behind the slits after many discrete photons impact, as if each particle is passing through both slits and interfering with itself. We find that the distribution of the trajectory end points of the APTs is in agreement with the pattern measured by ICCD. The helical APTs of single twisted photons help us to understand the optical manipulations of OAM and enable new applications in quantum imaging and sensing[25].

We firstly begin with the theoretical analysis, and the equation describing APTs is[26,27]

$$\frac{\mathrm{d}\mathbf{r}}{\mathrm{d}s}=\frac{1}{c}\frac{\mathbf{S}(\mathbf{r})}{U(\mathbf{r})}, \tag{1}$$

where $\mathbf{r}$ is the streamlines, s is a certain arc length of the corresponding trajectory, and c is the speed of light in vacuum. $\mathbf{S}(\mathbf{r})$ is the real part of the time-averaged Poynting vector carrying electromagnetic energy,

$$\mathbf{S}(\mathbf{r}) = \frac{1}{2}\mathrm{Re}[\mathbf{E}(\mathbf{r}) \times \mathbf{H}^*(\mathbf{r})], \tag{2}$$

and $U(\mathbf{r})$ is the energy density of a monochromatic electromagnetic field,

$$U(\mathbf{r}) = \frac{1}{4}[\varepsilon_0 \mathbf{E}(\mathbf{r}) \cdot \mathbf{E}^*(\mathbf{r}) + \mu_0 \mathbf{H}(\mathbf{r}) \cdot \mathbf{H}^*(\mathbf{r})], \tag{3}$$

where $\mathbf{E}(\mathbf{r})$ and $\mathbf{H}(\mathbf{r})$ are the spatial parts of the electric and magnetic fields of light, respectively. $\mathbf{E}(\mathbf{r}) = \psi(\mathbf{r})\hat{\mathbf{e}}$ ($\hat{\mathbf{e}}$ indicates the unit vector of polarization state); since the polarization state has no influence on APTs, here we only consider the scalar field. Let us consider the simplest example of a twisted light beam—a linearly polarized Laguerre–Gaussian beam propagating along the z axis (with a radial mode index $p = 0$)[28]:

$$\psi(\mathbf{r}) = \frac{\omega_0}{\omega(z)}\left[\frac{\sqrt{2}r}{\omega(z)}\right]^{|\ell|} \exp\left[\frac{ikr^2}{2R(z)} - \frac{r^2}{\omega^2(z)} + i\ell\phi + ikz\right], \tag{4}$$

where (r, ϕ, z) are cylindrical coordinates, ω_0 is the beam waist, $\omega(z) = \omega_0(1 + z^2/z_R)^{1/2}$ is the beam radius, $R(z) = (z^2 + z_R^2)/z$ is the curvature radius of the wavefront, and $z_R = k\omega_0^2/2$ ($k = 2\pi/\lambda$) is the Rayleigh diffraction range.

The distance between the centerlines of the two slits is $2a$. Behind the double slit, the superposition of the two twisted beams can be written as

$$\psi_0(\mathbf{r}) = \psi_1(\mathbf{r}_1) + \psi_2(\mathbf{r}_2) = \psi(r_1, \phi_1, z) + \psi(r_2, \phi_2, z), \tag{5}$$

where

$$r_1 = [(x - a)^2 + y^2]^{1/2}, \tag{6a}$$

$$r_2 = [(x + a)^2 + y^2]^{1/2}, \tag{6b}$$

$$\tan\phi_1 = \frac{y}{x - a}, \tag{6c}$$

$$\tan\phi_2 = \frac{y}{x + a}. \tag{6d}$$

Substituting Eqs. (5) and (6) into Eq. (1) for APTs, the simulated APTs of the twisted photons for the double-slit interference are shown in Fig. 1. We record the simulated three-dimensional structures of APTs for 1000 (500 initial points for each slit) photons in Fig. 1(a) and the two-dimensional structures in the xz plane for 60 trajectories in Fig. 1(b). From the APTs behind the double slit, we can intuitively see that the APTs exhibit helical structures. This is the reason why the twisted photon travels slower than the established speed of light[5]. Note that the APTs

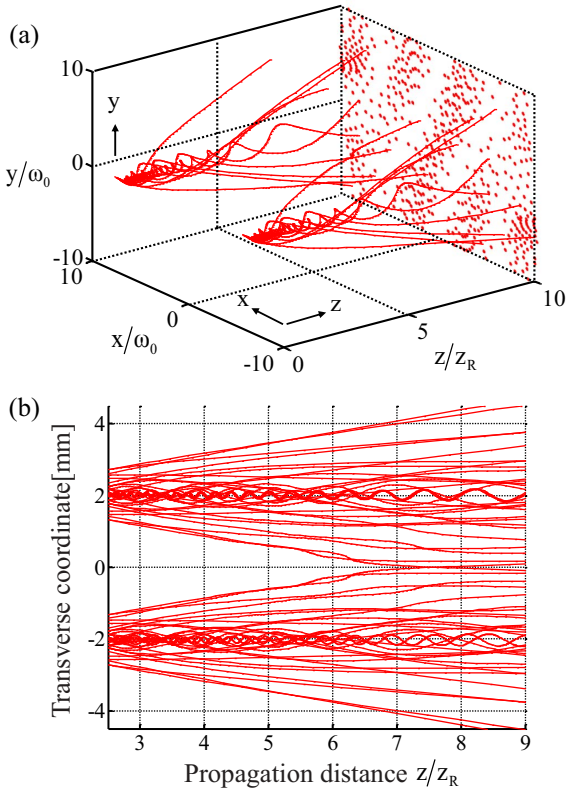

Fig. 1. The three-dimensional and two-dimensional APTs of the twisted light ($\ell = 1$) in the double-slit interference. (a) Three-dimensional structures and their projections at the $z = 10z_R$ plane (500 initial points for each slit). (b) Two-dimensional structures in the xz plane for 60 trajectories.

should not be identified with the actual path that a photon would follow[29]. The trajectories are the paths along which the electromagnetic energy flows, and ensembles of these trajectories will describe all of the eventual possible paths taken by any single photon[30].

Spontaneous parametric down-conversion (SPDC) is a well-known nonlinear optical process, in which one photon incident on a nonlinear crystal spontaneously splits into two photons. The experimental setup is shown in Fig. 2. We use a half-wave plate (HWP) and a broadband polarization beam splitter (PBS) to control the intensity of the pump laser, which is a horizontally polarized, single-mode, continuous-wave diode laser at a wavelength of 405 nm with a power of ~1 mW, and the inferred production rate of down-converted beams is $\sim 3 \times 10^5\ \mathrm{s}^{-1} \cdot \mathrm{mW}^{-1}$. The pump laser is focused by a lens with a focal length of 100 mm to pump a nonlinear crystal, which is a 10-mm-long, type-II periodically poled potassium titanyl phosphate (PPKTP) crystal. The temperature of the PPKTP is controlled by a heating oven with a stability of ~0.1°C. Under the collinear phase matching condition, the degenerate down-converted photon pairs are generated at a wavelength of 810 nm. The SPDC photon pairs are collimated by a lens with a focal length of 100 mm. The 3 nm narrow bandwidth interference filters (IFs) (centred at a wavelength of 810 nm) are used to improve the spectral purity

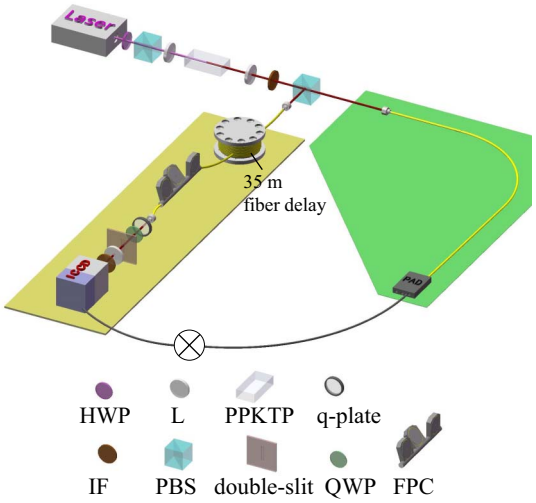

Fig. 2. Schematic diagram of experimental setup. HWP, half-wave plate; PBS, polarization beam splitter; L, lens; PPKTP, periodically poled KTP; IF, interference filter; QWP, quarter wave plate; FPC, fiber polarization controller; PAD, photon avalanche detector.

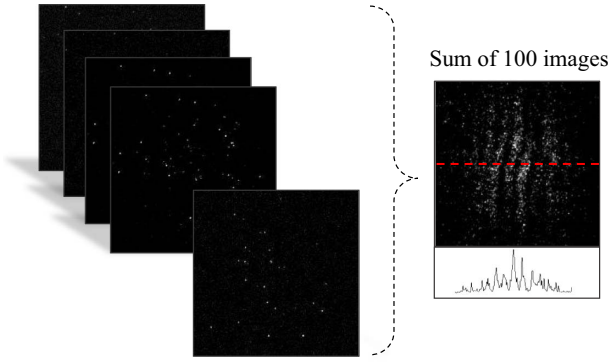

Fig. 3. Examples of 100 triggered coincidence images of $\ell = +1$ OAM photons by the ICCD camera and the summing pattern of 100 frame images. Every acquired frame has an exposure time of 100 ms and is photon sparse.

of the correlated photon pairs and to block the remaining pump laser. A PBS divides the signal and idler photons into two different paths. In the signal path, we use a pig-tailed single-photon avalanche detector (SPAD) without cooling with a response time of ~15 ns, as the heralding detector, to detect the signal photons as the external trigger of ICCD. However, here the ICCD is air cooled to −30°C. The ICCD triggering mechanism leads to an electronic delay of ~70 ns. Thus, there is a total electronic delay of ~85 ns.

In the idler path, a q-plate with $q = 1/2$ is used to generate the photons carrying OAM. The q-plate can convert a left-handed circularly polarized photon into a right-handed circularly polarized one with an $\ell = +2q$ OAM, while it can convert a right-handed circularly polarized photon into a left-handed circularly polarized one with an $\ell = -2q$ OAM[31]. Therefore, we use a fiber polarization controller (FPC) to adjust the polarization of the idler photons into left-handed circular polarization. Then, we used a lens with a focal length of 11 mm to collimate the beam coming out of the fiber, and the diameter of the collimated beam is about 2.1 mm. Behind the q-plate ($q = 1/2$), the right-handed circularly polarized idler photons with $\ell = +1$ OAM pass through a quarter wave plate (QWP) to become linearly polarized photons with $\ell = +1$ OAM. Meanwhile, we set the intensifier gate width at a 5 ns coincidence gate time to ensure that only the idler photon events are registered[32]. In order to guarantee that the photons detected at the heralding detector and at the ICCD camera are from the same correlated photon pair, we must introduce a 35 m single-mode fiber (SMF) (corresponding to ~175 ns) to compensate for the electronic delay of ~85 ns as mentioned above. Clearly, we over compensate for a time delay of ~90 ns (175–85 ns), which will be cancelled by introducing an electronic delay of ~90 ns by the ICCD-provided electronic system. Besides the gate width, there is another timing measure of note in an ICCD: the exposure time, which determines the accumulated time of the signal on the chip before it is read out. At first, we adjust the exposure time to be 100 ms (for each image) to ensure that each acquired frame is photon sparse[33], which leads to only about dozens of single-photon events. When only one image is studied, only a few scattering photons can be found, but no specific pattern can be recorded, because there are not enough detected photons to display the image. However, when summing many images, the pattern and its superposition can be recovered. Figure 3 shows the sum of 100 triggered coincidence images of $\ell = +1$ OAM photons with 100 ms exposure time. Summing these images means averaging many single-photon events. So, we can find that the summing pattern is consistent with the simulated result based on Poynting vector theory in Fig. 1(a).

The wave character of twisted photons will be obvious by extending the exposure time, because the number of registered photon events per image grows as the exposure time increases. Figure 4(a) shows the recorded images of the $\ell = +1$ twisted photons for different exposure times. As is well known, the observed intensity patterns occur as a consequence of photon statistics. If photons are detected one by one, the photons appear to be distributed quite randomly at first. The distribution behaviour of a large number of photons will be similar to the classical donut pattern. Of course, it is well established that photons exhibit the phenomenon of wave-particle duality in the double-slit interference, as shown in Fig. 4(b), and the two slits used here had the same width of 100 μm and a center-to-center separation of 500 μm. As the total number of accumulated photons increases, the bent interference fringes appear. We find that even if there are few photons, which have not been considered as electromagnetic energy flows, the phenomenon is the same as that of a large number of photons. The APTs can provide theoretical guidance for us to understand some phenomena in quantum to a certain extent, and provide us with more visual and intuitive understanding of quantum physics.

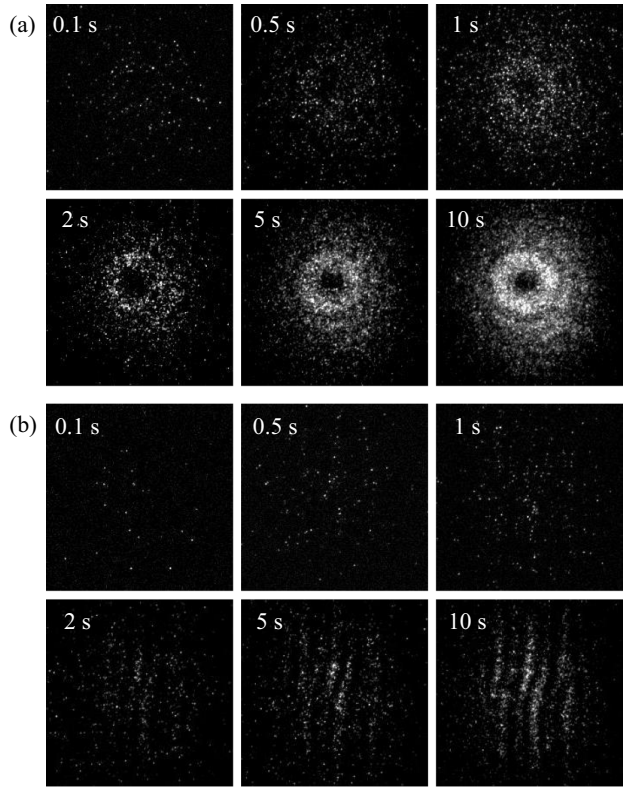

Fig. 4. Triggered images by the ICCD for different exposure times, for the $\ell = +1$ OAM twisted photons. (a) The $\ell = +1$ OAM twisted photons themselves and (b) in the double-slit interference. If the photons are detected one by one, the photons appear to be distributed quite randomly. As the total number of accumulated photons increases, the interference fringes appear.

In summary, we provided a classical-like method to describe the microscopic behaviour of photons. We theoretically predicted the APTs in the double-slit interference of single twisted photons, which still go along helical trajectories. Then, we experimentally obtained the low noise diffraction patterns by using the time-gated ICCD camera, which is triggered by a heralded detection. We demonstrated Young's interference of twisted photons at the single-photon level and the interference of each photon with itself supported by the heralded detection. The interference patterns obtained from averaging many single-photon events correspond to the distributions of the end points of APTs. The average trajectories can also offer a method to explore the microscopic behaviour of other quantum particles.

This work was supported by the National Key R&D Program of China (Nos. 2017YFA0303800 and 2017YFA0303700), the National Natural Science Foundation of China (Nos. 11534006, 11674184, and 11774183), the Natural Science Foundation of Tianjin (No. 16JCZDJC31300), and the Collaborative Innovation Center of Extreme Optics.

References

1. L. Allen, M. W. Beijersbergen, R. J. C. Spreeuw, and J. P. Woerdman, Phys. Rev. A **45**, 8185 (1992).
2. G. Gibson, J. Courtial, M. J. Padgett, M. Vasnetsov, V. Pasko, S. M. Barnett, and S. Franke-Arnold, Opt. Express **12**, 5448 (2004).
3. W. Zhang and L. Chen, Chin. Opt. Lett. **16**, 030501 (2018).
4. M. Malik, M. Erhard, M. Huber, M. Krenn, R. Fickler, and A. Zeilinger, Nat. Photon. **10**, 248 (2016).
5. F. Bouchard, J. Harris, H. Mand, R. W. Boyd, and E. Karimi, Optica **3**, 351 (2016).
6. S. Barz, E. Kashefi, A. Broadbent, J. F. Fitzsimons, A. Zeilinger, and P. Walther, Science **335**, 303 (2012).
7. J. Wang, J.-Y. Yang, I. M. Fazal, N. Ahmed, Y. Yan, H. Huang, Y. Ren, Y. Yue, S. Dolinar, M. Tur, and A. E. Willner, Nat. Photon. **6**, 488 (2012).
8. P. Grangier, G. Roger, and A. Aspect, Europhys. Lett. **1**, 173 (1986).
9. V. Jacques, E. Wu, T. Toury, F. Treussart, A. Aspect, P. Grangier, and J.-F. Roch, Eur. Phys. J. D **35**, 561 (2005).
10. J. Steeds, P. G. Merli, G. Pozzi, G. Missiroli, and A. Tonomura, Phys. World **16**, 20 (2003).
11. A. Zeilinger, R. Gahler, C. G. Shull, W. Treimer, and W. Mampe, Rev. Mod. Phys. **60**, 1067 (1988).
12. O. Camal and J. Mlynek, Phys. Rev. Lett. **66**, 2689 (1991).
13. O. Nairz, M. Arndt, and A. Zeilinger, Am. J. Phys. **71**, 319 (2003).
14. P. Shadbolt, J. C. F. Mathews, A. Laing, and J. L. O'Brien, Nat. Phys. **10**, 278 (2014).
15. M. O. Scully, B. G. Englert, and H. Walther, Nature **351**, 111 (1991).
16. Y. H. Kim, R. Yu, S. P. Kulik, Y. Shih, and M. O. Scully, Phys. Rev. Lett. **84**, 1 (2000).
17. H. Schouten, N. Kuzmin, G. Dubois, T. Visser, G. Gbur, P. Alkemade, H. Blok, D. Lenstra, and E. Eliel, Phys. Rev. Lett. **94**, 053901 (2005).
18. S. Kocsis, B. Braverman, S. Ravets, M. J. Stevens, R. P. Mirin, L. K. Shalm, and A. M. Steinberg, Science **332**, 1170 (2011).
19. R. Menzel, D. Puhlmann, A. Heuer, and W. P. S. Chleich, PNAS **109**, 9314 (2012).
20. E. Bolduc, J. Leach, F. M. Miatto, G. Leuchs, and R. W. Boyd, PNAS **111**, 9314 (2014).
21. D. H. Mahler, L. Rozema, K. Fisher, L. Vermeyden, K. J. Resch, H. M. Wiseman, and A. Steinberg, Sci. Adv. **2**, e11501466 (2016).
22. A. S. Rab, E. Polino, Z.-X. Man, N. B. An, Y.-J. Xia, N. Spagnolo, R. L. Franco, and F. Sciarrino, Nat. Commun. **8**, 915 (2017).
23. Y. Aharonov, D. Z. Albert, and L. Vaidman, Phys. Rev. Lett. **60**, 1351 (1988).
24. K. Y. Bliokh, A. Y. Bekshaev, A. G. Kofman, and F. Nori, New J. Phys. **15**, 073022 (2013).
25. Z. Gu, X. Wang, J. Wang, F. Fan, and S. Chang, Chin. Opt. Lett. **17**, 121103 (2019).
26. A. S. Sanz, M. Davidovic, M. Bozic, and S. Miret-Artés, Ann. Phys. **325**, 763 (2010).
27. Y. Li, Z. C. Ren, L. J. Kong, C. Tu, and H. T. Wang, Phys. Rev. A **95**, 043830 (2017).
28. H. I. Sztul and R. R. Alfano, Opt. Lett. **31**, 999 (2006).
29. A. B. Nassar and S. Miret-Artes, Phys. Rev. Lett. **111**, 150401 (2013).
30. M. Davidović, A. S. Sanz, D. Arsenović, M. Bozić, and S. Miret-Artés, Phys. Scr. **T135**, 014009 (2009).
31. L. Marrucci, C. Manzo, and D. Paparo, Phys. Rev. Lett. **96**, 163905 (2006).
32. R. Lapkiewicz, S. Ramelow, R. Fickler, M. Krenn, and A. Zeilinger, Sci. Rep. **3**, 1914 (2013).
33. D. Tasca, R. Aspden, P. Morris, G. Anderson, R. Boyd, and M. Padgett, Opt. Express **21**, 30460 (2013).